Asian Journal of Chemistry; Vol. 37, No. 12 (2025), 3147-3157
ASIAN JOURNAL OF CHEMISTRY
https://doi.org/10.14233/ajchem.2025.34814

Valorization of Food Waste as an Eco-Friendly Adsorbent for the Removal of Cationic Textile Dye from Aqueous Solutions: Kinetic, Isotherm and Thermodynamic Studies

SARA MEFTAH[1], FATIMA ZOHRA BATANA[2], SALIMA MERGHACHE[1,3,*], LILA BOUZINA[1] and MUTLU SÖNMEZ ÇELEBI[4]

[1]Laboratory of Inorganic Chemistry and Environment (LCIE), Department of Chemistry, Faculty of Sciences, University of Tlemcen, P.O. Box 119, Tlemcen 13000, Algeria
[2]Laboratory of Physical Chemistry of Materials (LPCM), Department of Process Engineering, Faculty of Technology, University of Laghouat, P.O. Box 37 G, Laghouat, Algeria
[3]Laboratory of Functional Agrosystems and Technology of Agronomic Sectors, Department of Agronomy, Faculty of Nature and Life Sciences and Earth and Universe Sciences, Tlemcen University, Imama, Tlemcen 13000, Algeria
[4]Department of Chemistry, Faculty of Science and Arts, University of Ordu, 52200, Ordu, Turkey

*Corresponding author: E-mail: salima.merghache@univ-tlemcen.dz

Received: 1 September 2025 *Accepted*: 12 November 2025 *Published online*: 30 November 2025 AJC-22206

In this study, *Helix aspersa* snail shells, a type of food waste and an effective adsorbent, were used to remove methyl violet 2B, a cationic dye commonly found in textile industry wastewater. This adsorbent is cost-effective, environmentally friendly, widely available and highly efficient. The characterization of the material was carried out using several techniques including SEM/EDX, XRD, TGA/DTA and FTIR, to provide a comprehensive analysis of the material's properties. SEM/EDX analysis showed a heterogeneous morphology of this adsorbent, while XRD confirmed that the main component was $CaCO_3$. After optimizing operational parameters, the highest removal efficiency (93.6%) was achieved at an initial dye concentration of 10 ppm, with particle size less than 0.1 mm, an adsorbent mass of 1.5 g, pH 8, an agitation speed of 700 rpm at a temperature of 20 ºC. The results showed a decrease in removal efficiency with increased ionic strength, with efficiency dropping to 49.5% at NaCl 1 M. The kinetic studies suggested that the adsorption followed a pseudo-second-order model. The adsorption isotherms were best described by the Langmuir model, suggesting monolayer adsorption on a surface with identical sites. Thermodynamic analysis revealed that the phenomenon was exothermic and spontaneous indicating that it is a physisorption process.

Keywords: Methyl violet 2B, Food waste, Snail shell, Wastewater, Adsorption, Kinetic, Isotherms, Thermodynamic studies.

INTRODUCTION

Wastewater from various industrial sectors is contaminated with dyes that pose significant environmental and health risks. Beyond causing visual pollution, these substances infiltrate natural water bodies such as rivers, streams and oceans, leading to significant ecological damage. Each year, over 700,000 tons of synthetic dyes are produced globally, with more than 10,000 different types used in industrial processes. This results in the release of approximately 5,000 tons of dyeing materials into the environment annually. Such large-scale discharge degrades water quality, harms aquatic life and raises concerns about potential human health impacts [1-4].

Dyes, such as methyl violet 2B (MV2B), are complex molecules known for their resistance to light, oxidants and temperature. MV2B is widely used in various industries to impart deep shades to materials such as wool, cotton, bamboo, silk, straw, paper and leather [2]. Furthermore, it is employed as an antiallergen and bactericide, however, it poses a threat to human health, with potential effects such as digestive system irritation, sleepiness, allergic dermatitis, genetic mutations and even or immunosuppressive responses [5-7].

In addition to its health impacts, this dye reduces dissolved oxygen levels in water, limit sunlight penetration and disrupt photosynthesis, contributing to eutrophication and the degradation of aquatic ecosystems [2]. As a result, removing it from wastewater has become a major focus of this research. Various treatment techniques have been developed including osmosis, ozonization, chemical precipitation, fungal degradation, ion exchange, adsorption, membrane filtration, coagulation,

flocculation, electrochemical and photodegradation methods [8-10]. Among these, adsorption remains one of the most efficient, cost-effective and user-friendly techniques for treating dye-laden effluents [11]. The process involves transferring contaminants from a liquid phase to the surface of the adsorbent with its efficiency largely dependent on the interactions between the adsorbent and the pollutants [12]. Recently, there has been growing interest in using natural biomass, both plant and animal based, for wastewater treatment due to its biodegradability, availability and environmental benefits. Natural adsorbents such as fruit peels, snail shells, peat, rice husks, clay, charcoal and plant waste, have emerged as promising alternatives for pollutants removal [8,13-16].

Among these, snail shells, a common form of food waste, are of particular interest due to their high calcium carbonate content. Owing to this composition, they have been investigated as cost-effective and sustainable bioadsorbents for removing a wide range of dyes, including malachite green oxalate, alizarin red, methylene blue and safranine [8,12,17,18].

This study specifically focuses on *Helix aspersa* snail shells, a common food waste byproduct and the most widespread species in Algeria and North Africa. It aims to investigate their potential as a biosorbent for removing MV2B from aqueous solutions. According to the literature review, no information is available regarding the utilization of snail shells as biosorbent for removing the MV2B dye. The material will be characterized using techniques such as infrared spectroscopy (IR), X-ray diffraction (XRD), scanning electron microscopy (SEM), energy dispersive X-ray (EDX) and thermogravimetric analysis/differential thermal analysis (TGA/DTA). The impact of various operational parameters, including particle size, adsorbent mass, initial pH, ionic strength, temperature, agitation speed, contact time and initial dye concentration, will be evaluated to optimize dye removal efficiency. Moreover, the experimental data will be analyzed using kinetic models such as pseudo-first-order, pseudo-second-order and intraparticle diffusion, while equilibrium data will be fitted to Langmuir, Freundlich and Temkin isotherms. Thermodynamic parameters will also be investigated to better understand the adsorption process.

EXPERIMENTAL

Hydrochloric acid (HCl), sodium hydroxide (NaOH) and sodium chloride (NaCl) were all purchased from Sigma-Aldrich and used without further purification. All chemicals were of analytical reagent grade.

Adsorbent material: The snail (*Helix aspersa*) shells were collected locally from a small restaurant in Bab El Assa, Tlemcen province in northwestern Algeria, washed with tap water, then rinsed with distilled water and finally dried before being ground in an electric grinder. The powder was sieved using laboratory sieves with known mesh sizes of 0.1 mm, 0.2 mm, 0.5 mm in order to obtain a powder of different grain size. The snail shell powder (SS) was dried in an oven at 50 ºC and then stored in a desiccator to be used for the characterization and the batch adsorption experiments.

Adsorbate material: Methyl violet 2B ($C_{24}H_{28}N_3Cl$) was purchased from Fluka AG, chemischefabrik. A stock solution of 1000 mg/L of MV2B was prepared for calibration purposes. From the stock, different concentrations of MV2B were prepared by diluting with distilled water. The calibration curve was plotted from the dye solution prepared in the concentration range of 0.1 to 10 mg/L. MV2B dye in the aqueous solution was analyzed using JENWAY 7300 UV-visible spectrophotometer at 580 nm.

Characterization of adsorbent material (SS)

pH at the point of zero charge: pH at the point of zero charge (pH_{pzc}) for the adsorbent was determined by pH drift method [6]. Sodium chloride (0.1 M) solution was used as an inert electrolyte. Initial pH values ($pH_{initial}$) of the NaCl solutions were adjusted from 1 to 11 by adding carefully the required amount of solution either 0.1 M HCl or 0.1 M NaOH using a micropipette. Adsorbent (0.1 g) was added into 50 mL of 0.1 M NaCl solution. The suspension mixture was allowed to equilibrate for 24 h in a shaker maintained at room temperature. Then, the suspension solution was filtered and the pH values (pH_{final}) were measured.

The $\Delta pH = pH_{final} - pH_{initial}$ of all solutions, were plotted against initial pH to calculate pH_{pzc}. The $pH_{initial}$ in which the curve crosses the $\Delta pH = 0$ line is considered as values of pH_{pzc} of the adsorbent at room temperature.

Characterization: The functional groups on the adsorbent's surface were identified using Fourier transform infrared (FTIR) (Perkin-Elmer spectrophotometer) in the scanning range of 4000-450 cm^{-1} using KBr pallets. The XRD studies were carried out on an X-ray powder diffractometer Rigaku Mini Flex 600 at 40 kV and 15 mA with Cu*K*α radiation. The morphological surface analysis of adsorbent as well as for the presence of elemental information on the samples, the EDX analyses the samples were studied by field emission gun-based scanning electron microscope with energy dispersive X-ray (SEM/EDX) technique. EDX spectra were taken from the area corresponding to the SEM image shown in the inset. The SEM studies were performed at 30 kV in the low vacuum mode, with a take-off angle of 35º. The thermogravimetric analysis (TGA) was performed using the Labsys Evo instrument. Approximately 10 mg of the desired precursor specimen was placed in an alumina (Al_2O_3) crucible at the end of a rod suspended from the arm of a balance with a sensitivity of 0.02 µg and a drift of less than 0.2 µg.

Batch adsorption studies: Batch adsorption experiments were carried out by mixing 75 mL of known concentration of MV2B solution (10 mg/L) with 0.25 g of adsorbent in a 250 mL conical flask. The mixtures were then agitated for 180 min on an orbital shaker at 500 rpm. The tests are carried out at room temperature (≈ 20 ºC) and at pH of the solution (pH ≈ 6). Various parameters were studied to optimize the experimental conditions, including the particle size of the snail shell (SS) adsorbent (≤ 0.1-0.5 mm), adsorbent mass (0.05-1.5 g), agitation speed (0-1000 rpm), medium pH (2-11), temperature (10-50 ºC), ionic strength (0-1.0 mol/L), contact time (1-180 min) and initial dye concentration (10-80 mg/L). The medium pH was adjusted using aqueous solutions of HCl and NaOH 1 M. In each experiment, the testing procedure was carried out under the condition that only one variable was modified at a time while the others remained constant. After each adsorption process, the samples were centrifuged (5000 rpm, 10 min) for

solid-liquid separation and the residual dye concentration in solution was analyzed by a UV-visible spectrophotometer (7300 JENWAY) at 580 nm wave length. The removal percentage (R, %) and the amount of MV2B adsorbed at time t (q_t, mg/g) were calculated by applying eqns. 1 and 2, respectively:

$$R\ (\%) = \left(\frac{C_o - C_t}{C_o}\right) \times 100 \quad (1)$$

$$q_t = \left(\frac{C_o - C_t}{m}\right) \times V \quad (2)$$

where C_o is the initial dye concentration (mg/L); C_t is the dye concentration at the time t (mg/L); V is the volume of MV2B solution used (L); and m is the mass of the adsorbent used (g).

RESULTS AND DISCUSSION

Characterization of SS

Point of zero charge pzc: The surface acidity and basicity are important criteria describing the surface chemistry of the adsorbents. The combined influence of all the functional groups of adsorbents determines pH_{pzc}. As a way to better understand the influence of pH on dye removal, the point of zero charge of the SS surface has been established. The dye removal is maximal depending on interaction between the cations and the surface of a material which is favoured at pH > pH_{pzc}. In contrast, at pH < pH_{pzc}, the interaction of anions is favoured. Fig. 1 shows that pH_{pzc} of SS is 8.24 at ΔpH = 0. This shows that the surface of the SS is predominated by positive charges at pH less than 8.24. However, the surface is predominated by negative charges if the pH higher than 8.24. A value of 8.5 has been reported as the pH for the zero point of charge of SS in results of Zhao *et al.* [19].

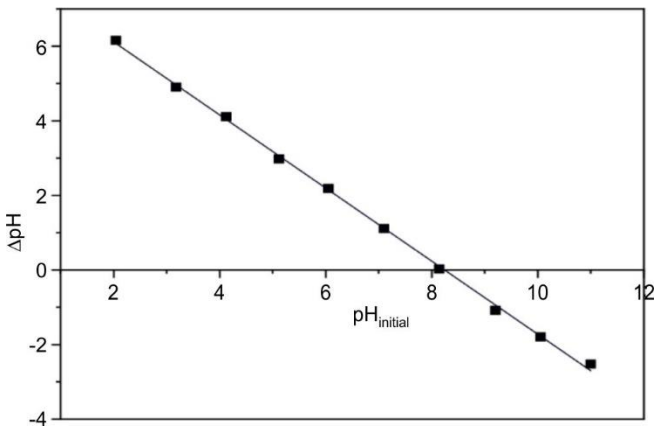

Fig. 1. Plot of point zero charge of the adsorbent SS

FTIR analysis: The FTIR spectra before and after MV2B adsorption onto SS are shown in Fig. 2. In the spectrum of SS before adsorption (Fig. 2a), a broad peak around 3439 cm^{-1} is attributed to the vibration of O–H stretching. A strong band at 2922 cm^{-1} is due to C–H stretching frequency. The peaks at approximately 1473 cm^{-1}, 1385 cm^{-1}, 861 cm^{-1}, 713 cm^{-1} and 700 cm^{-1} are attributed to the carbonate group's C-O stretching vibration. The characteristic bands at 2583 cm^{-1}, 1789 cm^{-1} and 1083 cm^{-1} involved the stretching vibration of

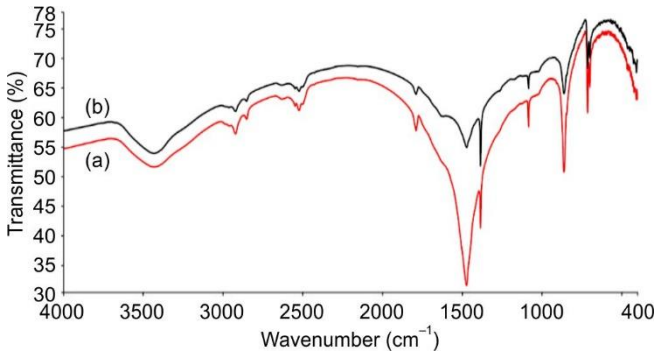

Fig. 2. FTIR spectra of SS before (a) and after (b) adsorption of MV2B

C=O groups of carbonate ion. This further confirms that $CaCO_3$ is the major constituent of SS powder. The FTIR spectrum of MV2B loaded SS (Fig. 2b) shows the distinct shift in certain bands as well as changes in intensity [20]. These observations suggest interactions between the MV2B molecules and the functional groups of SS during adsorption.

XRD analysis: The X–ray diffraction profiles for SS before and after MV2B adsorption are shown in Fig. 3, which presents the small angle XRD patterns of the samples. The XRD pattern of SS (Fig. 3a) displays several diffraction peaks in the 2θ range of 20-80º. These peaks are well indexed to a calcium carbonate polymorph, primarily indicating a highly crystalline aragonite structure. After adsorption (Fig. 3b), the XRD pattern of MV2B-loaded SS shows no significant change in the crystalline structure. This suggests that MV2B molecules likely diffuse into the micropores and macropores of the material and are adsorbed mainly through physisorption, without altering the structural integrity of the adsorbent [21].

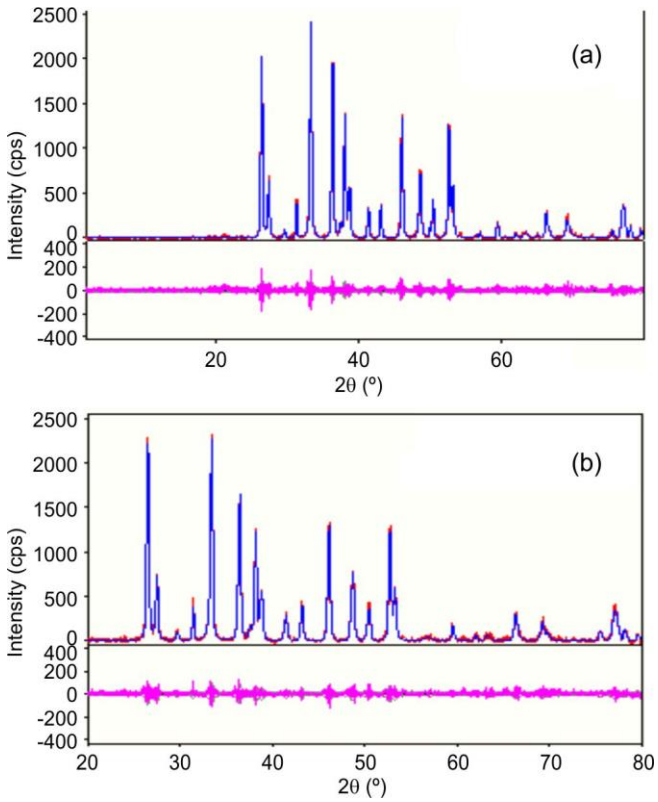

Fig. 3. XRD patterns of SS before (a) and after (b) adsorption of MV2B

SEM/EDX analysis: Figs. 4 and 5 present the results of SEM and EDX analysis of SS before and after adsorption, respectively. The SEM images (Fig. 4) reveal that SS exhibits a stratified lamellar surface and an irregular morphological structure of particles with smaller sizes. The dark regions observed on the surface may be attributed to the presence of carbon rich strands. For the MV2B adsorption onto SS, similar features have been reported, suggesting that sorption by the $CaCO_3$ compound often follows surface precipitation due to the identical ionic radii of divalent calcium and MV2B [22]. However, EDX analysis in Fig. 5, shows that SS predominantly contains calcium, with different amounts of other elements such as carbon, iron, oxygen, magnesium, sodium, aluminum and silicon.

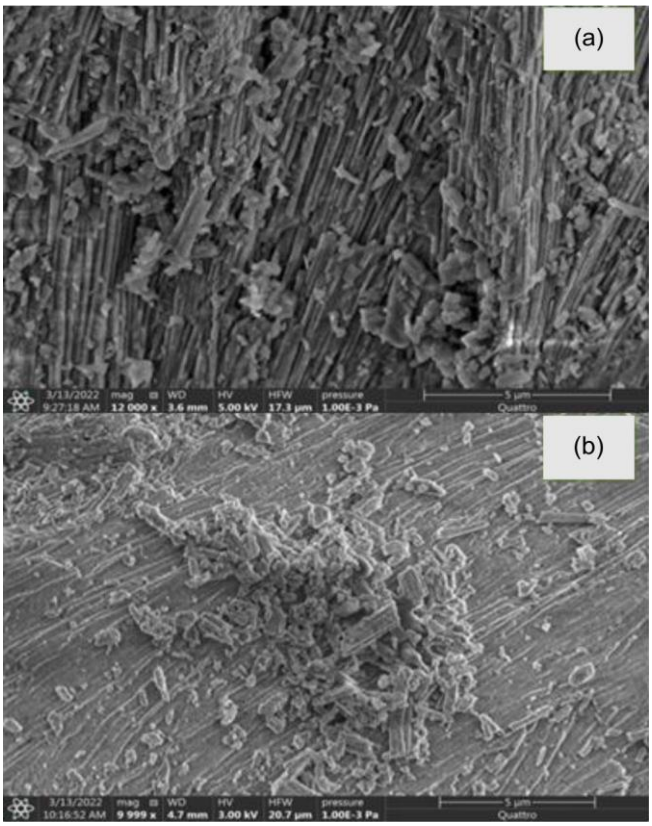

Fig. 4. SEM micrographs of SS before (a) and after (b) adsorption of MV2B

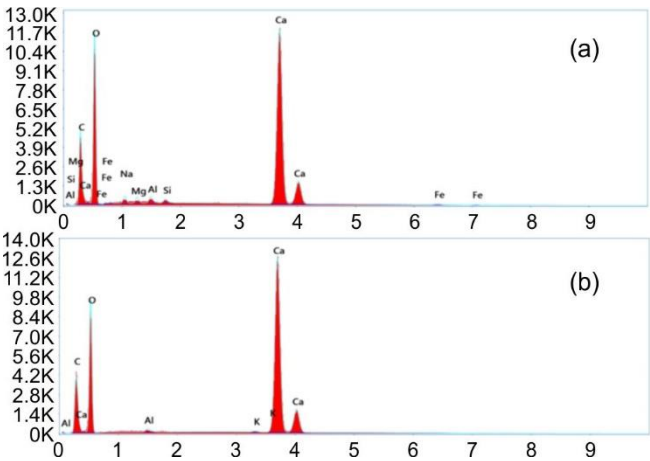

Fig. 5. EDX spectra of SS before (a) and after (b) adsorption of MV2B

Thermal studies: The TGA and DTA curves of SS were illustrated in Fig. 6. Between 50 ºC and 565 ºC, a minor weight reduction was observed, attributed to the evaporation of water molecules and organic compounds. Between 565 ºC and 831 ºC, a notable shift in weight was observed, primarily due to the beginning of the decomposition of $CaCO_3$ into CaO, accompanied by the release of CO_2. Beyond 831 ºC, the weight of the snail shell material reached stability, indicating the completion of the $CaCO_3$ decomposition process into CaO. The same result was obtained by Laskar *et al.* [23].

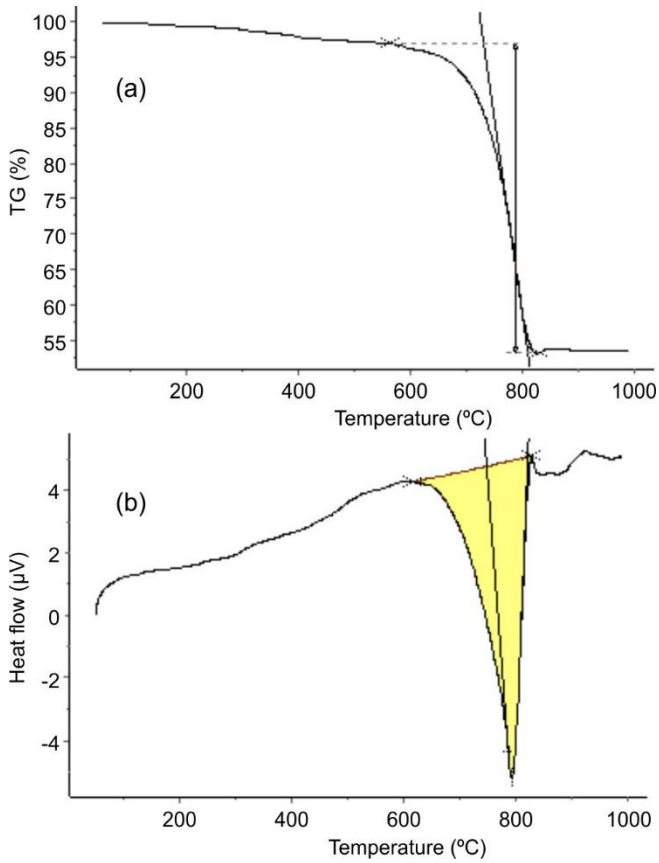

Fig. 6. TGA/DTA analysis of SS

Preliminary adsorption studies

Effect of particle size: The variation in particle size of SS significantly affects the removal efficiency of MV2B. In this study, adsorption experiments were conducted using SS particles of different sizes (< 0.1 mm, 0.1 mm, 0.2 mm, 0.5 mm and raw material). The results, presented in Fig. 7, show that the removal efficiency of MV2B ranged from 76.7% for particles < 0.1 mm to 45.41% for particles of 0.5 mm. Adsorption efficiency increased with decreasing particle size and decreased with larger particles. This behaviour can be attributed to the higher surface area and greater density of active surface sites in smaller particles, which enhance surface retention capacity. Also, the smaller particles tend to exhibit a stronger affinity for contaminant retention [24].

Effect of adsorbent mass: The adsorbent dosage constitutes one of the essential factors in adsorption studies as it directly influences the adsorption capacity at a given initial dye concentration. The study was carried out using different

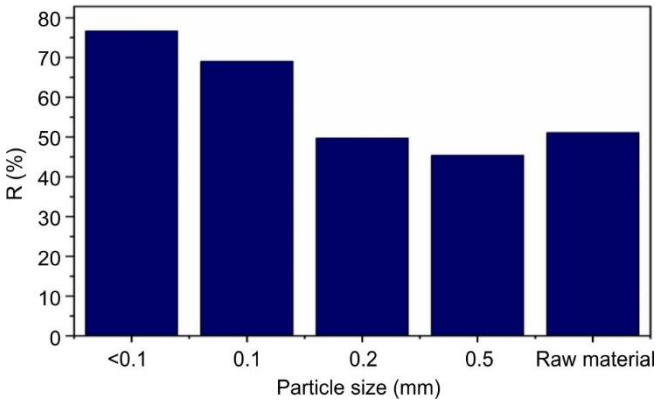

Fig. 7. Effect of particle size on percentage removal of MV2B dye by SS

adsorbent masses ranging from 0.05 to 1.5 g. The increase in dye removal to 86.97 % appears to be directly proportional to the rise in adsorbent mass to 1.5 g (Fig. 8). This can be attributed to the greater number of active sites available on the SS surface, which provides more binding opportunities for the dye [2,25]. Consequently, enhanced fixation of MV2B on the adsorption sites of SS is observed.

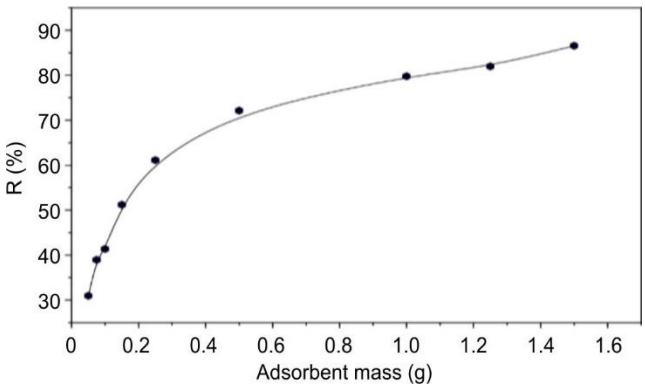

Fig. 8. Effect of adsorbent mass on percentage removal of MV2B dye by SS

Effect of initial pH: pH is a critical factor influencing dye adsorption, as it affects both the aqueous chemistry of the solution and the surface binding sites of the adsorbent. Each dye has an optimal pH for adsorption onto a specific adsorbent. The present study is based on changing the pH of the methyl violet solution from 2 to 11. It appears that the adsorption increased with the rise in pH, reaching a maximum of 78.29% at pH 8, but decreased when the pH was further increased (Fig. 9). At lower values of pH, the surface of the adsorbent acquires positive charges by absorbing H^+ ions, which prevent the adsorption of dye ions onto adsorbent surface due to electrostatic repulsion and the competition between H^+ ions and MV2B for the adsorption site. As the solution pH increases, the number of negatively charged surface sites on the adsorbent also increases, potentially leading to an increase in the adsorption of cationic dye molecules due to electrostatic attraction. The low dye removal at high pH (pH > 8) was due to the strong repulsion between the negatively charged adsorbent and deprotonated dye molecules [26].

Effect of ionic strength: The ionic strength of the solution plays a pivotal role in controlling both electrostatic and non-electrostatic interactions between the adsorbate and the

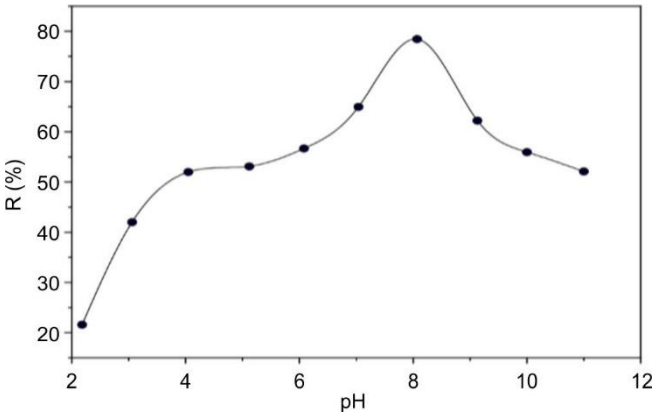

Fig. 9. Effect of initial pH of the solution on percentage removal of MV2B dye by SS

adsorbent surface. The effect of ionic strength on the adsorption of MV2B onto SS was investigated by varying NaCl concentrations from 0 to 1 mol/L, while maintaining a constant MV2B concentration of 10 mg/L. An increase in ionic strength led to a reduction in removal efficiency, decreasing from 74% to 49% (Fig. 10). This decline in removal efficiencies can be attributed to Cl^- ions, which act to shield electrostatic attrac-%tion between MV2B and SS material. In addition, excess Na^+ ions enter into competition with MV2B molecules for adsor-ption sites. Consequently, these findings suggest that the adsorption of MV2B onto SS particles is significantly influ-enced by the ionic strength of the dye solution, aligning with findings in several other studies [27].

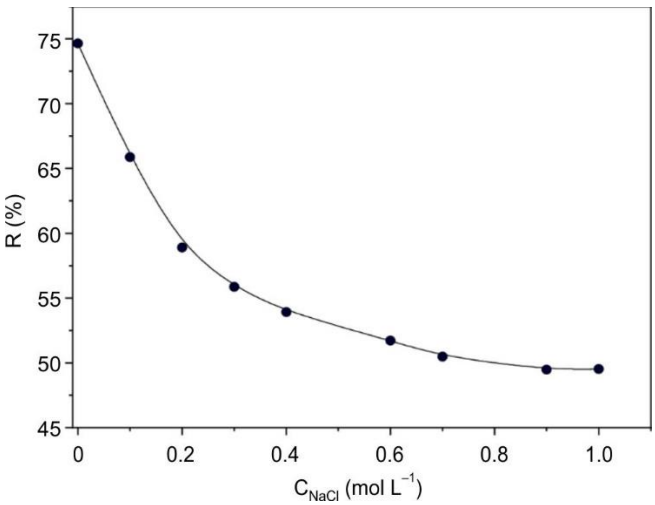

Fig. 10. Effect of ionic strength on percentage removal of MV2B dye by SS

Effect of temperature: The findings of MV2B removal at temperatures ranging from 10 to 50 ºC are shown in Fig. 11. As the temperature increased from 10 ºC to 20 ºC, the removal efficiency surged from 66.47% to 86.97%, indicating an endothermic nature of the adsorption process at lower temperatures. However, the subsequent rise in temperature from 20 ºC to 50 ºC resulted in a reduction in MV2B removal. This can be attributed to the weakening of physical bonding between the active sites of the adsorbent and the dye (adsorbate) as the temperature [2]. On the other hand, the interaction forces between the solvent and the solute are stronger than those

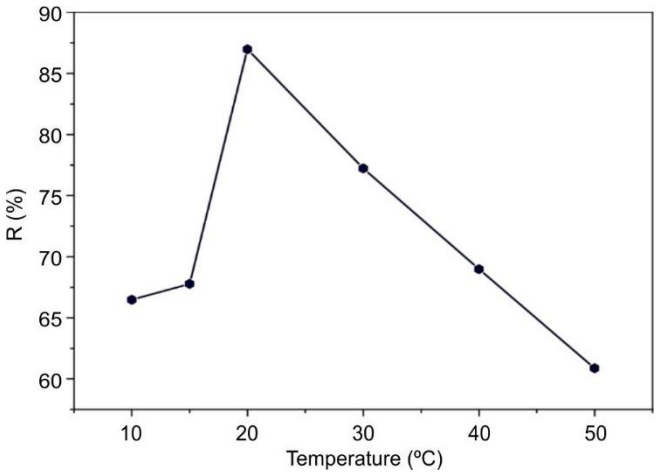

Fig. 11. Effect of temperature on percentage removal of MV2B dye by SS

between the adsorbent and the solute. As a result, the solute faces difficulties in adhering to the snail shell, since the predominant forces are those between the solute and the solvent, which overshadow the interactions between the solute and the adsorbent [28].

Effect of agitation speed: Fig. 12 indicate a significant increase in removal efficiency, peaking at 700 rpm with an efficiency of 63.31%. This rise in MV2B removal efficiency is attributed to improved contact between the biosorbent binding sites and the dye, facilitating the transport of dye ions to adsorbent sites. The enhanced yield is observed when the stirring rate of agitation equals 700 rpm, followed by a subsequent decrease from 700 rpm to 1000 rpm. For relatively high stirring speeds (≤ 700 rpm), the turbulence, which is induced by agitation, enhances the mass transfer of dyes from the bulk solution to the biomass surface, aiding in the fixation of dyes on the biomass surface and thereby improving the sorption process. Moreover, at very high speed (> 700 rpm), centrifugal forces operate, resulting in desorption of the adsorbate [28].

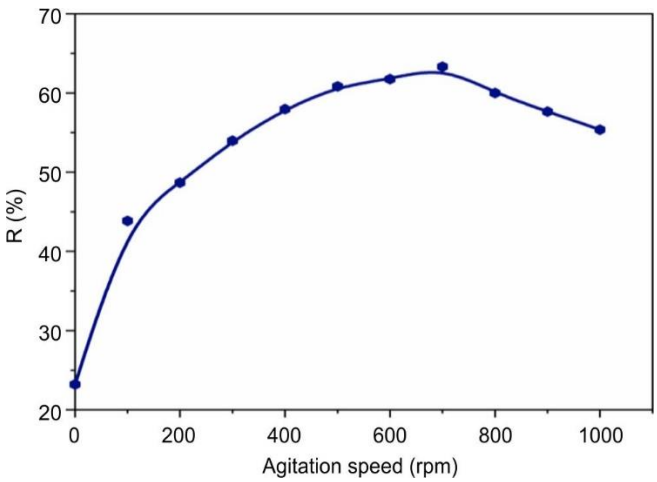

Fig. 12. Effect of agitation speed on percentage removal of MV2B dye by SS

Effect of contact time and initial dye concentration: The results shown in Fig. 13 indicate that as the initial dye concentration increased from 10 to 80 mg/L, the dye removal

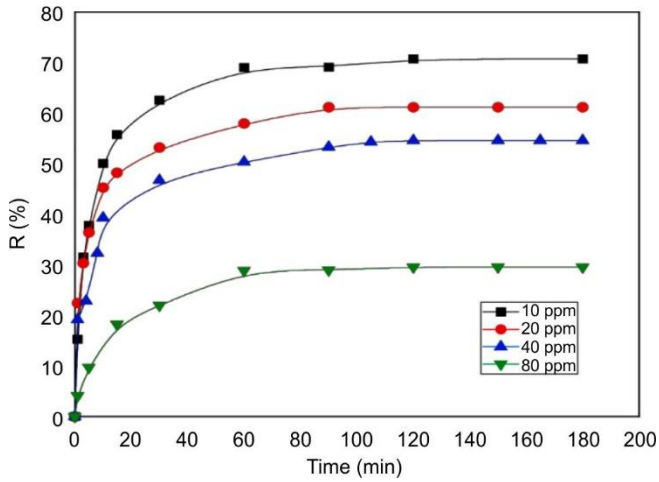

Fig. 13. Effect of contact time and initial dye concentration on percentage removal of MV2B dye by SS

percentage decreased from 69.43% to 27.22%. This reduction in removal efficiency at higher concentrations can be attributed to the higher amount of dye in the solution, where the amount of SS used was insufficient to achieve high removal rates at elevated concentrations [2]. Regarding contact time, the removal percentage (R) increased as the adsorption process progressed until equilibrium was reached. This is due to the growing interaction between the solute and the biosorbent, which initially leads to higher adsorption of MV2B onto the snail shell. As the available adsorption sites became occupied, the process slowed and efficiency decreased. Moreover, higher dye concentrations resulted in longer equilibrium times, which progressively increased to 60, 75, 90 and 110 min for concentrations of 10, 20, 40 and 80 ppm, respectively. This delay can be attributed to increased electrostatic repulsion between dye molecules in the solution, which enhances the resistance to mass transfer, though the effect is less noticeable at the interface, as a result, the adsorption process becomes slower [29].

Optimization of methyl violet removal under ideal operating conditions: The aim of this study is to evaluate the removal efficiency of methyl violet using snail shell powder under optimal operational conditions, including temperature (20 °C), agitation speed (700 rpm), pH (8), initial dye concentration (10 mg/L) and adsorbent dose (1.5 g). The results, presented in Fig. 14, demonstrate that the removal efficiency reached 60% within the first minute, indicating a rapid kinetic process. The removal efficiency of MV2B increased to 91.22% after 60 min and reached equilibrium. After 180 min, the removal efficiency further improved to 93.63%. These results suggest that snail shell powder is an excellent, cost-effective adsorbent for removing methyl violet.

Kinetics modeling: To investigate the removal of the dye MV2B by adsorption onto SS, three kinetic models have been studied *viz*. pseudo-first-order, pseudo-second-order and intraparticle diffusion. These models are most commonly used to describe the kinetic of sorption. The conformity between the experimental data and the model predicted values was expressed by the correlation coefficients (R^2) and the comparison of the value of q_e calculated with that determined experimentally.

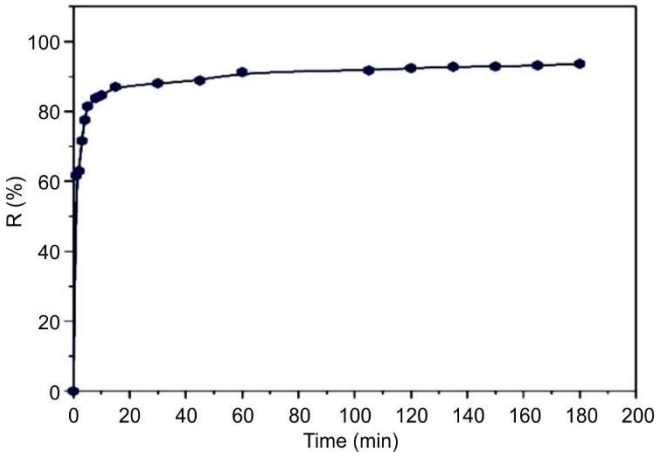

Fig. 14. Removal of MV2B dye by SS under optimal operating conditions

Pseudo-first-order kinetic model: The pseudo-first-order model was used to estimate the specific rate constant for adsorption [30]. It can be expressed following the Lagergren rate equation:

$$\ln (q_e - q_t) = \ln q_e - k_1 t \quad (3)$$

where q_e, q_t are the amounts of adsorbate adsorbed (mg/g) at equilibrium and at contact time t (min) respectively and k_1 is the pseudo-first-order rate constant (min^{-1}). The pseudo-first-order rate constant k_1 values and adsorption capacity q_e were calculated from the slope and the intercept of the plots of ln ($q_e - q_t$) *versus* t (Fig. 15). The k_1, q_e and R^2 values are recapped in Table-1. The correlation coefficients for the pseudo-first-order model ranged from 0.947 to 0.966. However, the calculated values q_{ecal} obtained from the linear plots did not correspond adequately with the experimental q_{eexp} values. This discrepancy indicates that the pseudo-first-order kinetic model did not accurately describe the kinetics of MV2B adsorption onto SS.

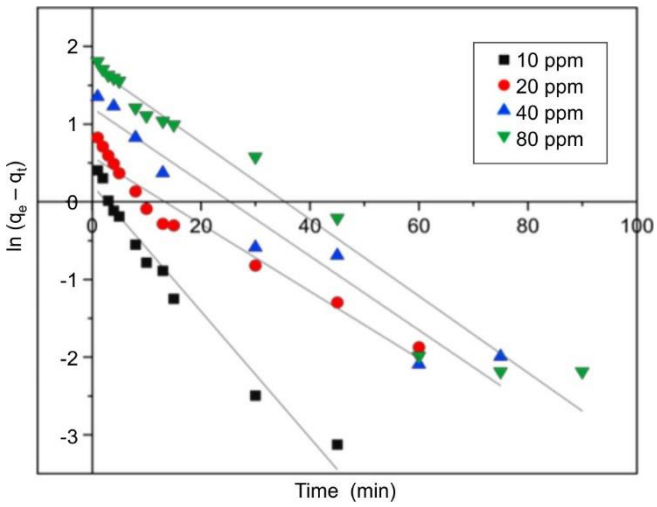

Fig. 15. The plots of pseudo-first-order kinetic model for adsorption of MV2B onto SS

Pseudo-second-order kinetic model: The pseudo-second-order model is presented by the following equation:

$$\frac{t}{q_t} = \frac{1}{k_2 q_e^2} + \frac{1}{q_e} t \quad (4)$$

where k_2 (g/mg.min) is the rate constant of the pseudo-second-order model. The q_e and k_2 values of the pseudo-second-order kinetic model can be determined from the slope and the intercept of the plots of t/q_t *versus* t (Fig. 16) [31]. The k_2, q_e and R^2 values are summarized in Table-1. The high correlation coefficients for the pseudo-second-order kinetic model, ranging from 0.997 to 0.999, indicate an excellent fit. Furthermore, the calculated adsorption capacities q_{ecal} obtained from the linear plots are in good agreement with the experimental values q_{eexp}. These findings suggest that the pseudo-second-order model best describes the adsorption kinetics of MV2B onto SS. Many similar results are found in the literature as those of Rahchamani *et al.* [32].

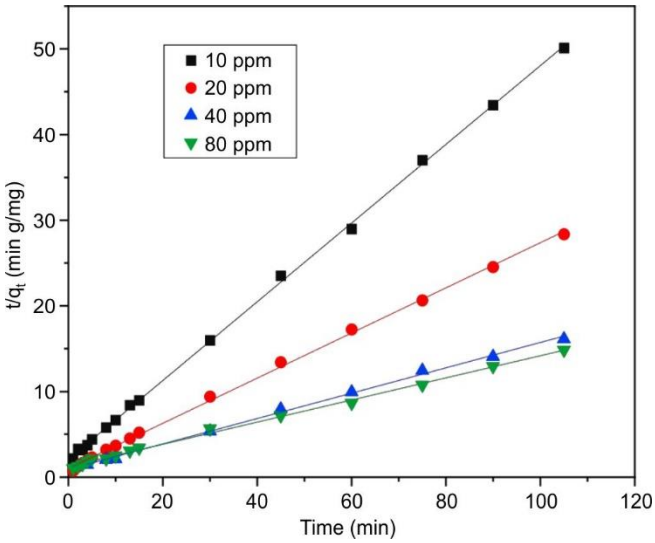

Fig. 16. The plots of pseudo-second-order kinetic model for adsorption of MV2B onto SS

Intraparticle diffusion: According to the Weber & Morris intraparticle diffusion model [33], sorption is a multi-step process where intraparticle diffusion can be the rate-limiting step, although other mechanisms like surface adsorption and internal diffusion also occur. Adsorption typically follows a

TABLE-1
KINETIC PARAMETERS OBTAINED AT DIFFERENT INITIAL CONCENTRATION FOR MV2B ADSORPTION ONTO SS

SS		Pseudo-first-order kinetic			Pseudo-second-order kinetic			Intraparticle diffusion model					
C_0	q_{eexp}	q_{ecal}	k_1	R^2	q_{ecal}	k_2	R^2	K_{i1}	K_{i2}	C_1	C_2	R_1^2	R_2^2
10	2.070	1.242	0.081	0.966	2.176	0.100	0.999	0.415	0.049	0.139	1.595	0.954	0.982
20	3.631	1.782	0.043	0.947	3.794	0.068	0.998	0.564	0.112	0.843	2.603	0.983	0.969
40	6.163	3.444	0.047	0.949	6.754	0.023	0.997	1.100	0.193	1.203	4.708	0.915	0.931
80	7.069	5.739	0.049	0.961	7.739	0.013	0.997	0.636	0.354	1.635	3.438	0.987	0.790

pattern where the uptake varies with the square root of time ($t^{1/2}$), expressed by the equation:

$$q_t = k_i t^{1/2} + C \quad (5)$$

where q_t is the dye uptake at time t, k_i is the intraparticle diffusion rate constant ; and C is the intercept indicating boundary layer thickness. By plotting q_t *vs.* $t^{1/2}$, two distinct linear phases appear (Fig. 17): (i) Phase 1 (macropore diffusion): rapid dye transfer to the outer surface (film diffusion); and (ii) Phase 2 (micropore diffusion): slower diffusion into pores.

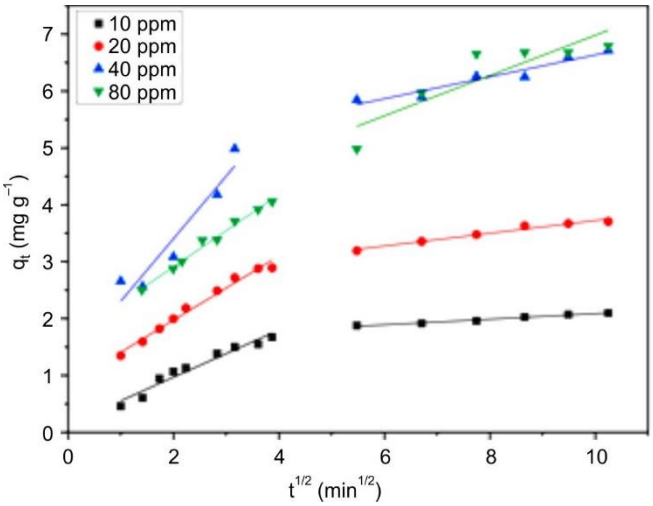

Fig. 17. The plots of intraparticle diffusion model for MV2B adsorption onto SS

The fact that the lines don't pass through the origin suggests that both film diffusion and intraparticle diffusion occur simultaneously. Larger C values (Table-1) imply a greater boundary layer effect. Similar results are found in the literature as that Doğan *et al.* [34] for the adsorption kinetics and mechanism of cationic dyes: methyl violet and methylene blue onto sepiolite and Mall *et al.* [35] for the removal of orange-G and methyl violet dyes by adsorption onto bagasse fly ash.

Equilibrium isotherm studies and modeling

Equilibrium isotherm: Fig. 18 presents the isotherm for the adsorption of MV2B onto SS. The equilibrium adsorption capacity q_e, increased with an increase in dye concentration, depending on the initial concentration of MV2B. Type I isotherms are characterized by horizontal plateau, it is the simplest case of adsorption, where the surface has identical elementary adsorption sites able to host single adsorbed molecule and it can be described by Langmuir equation [36].

Isotherms modelling: In this study, the Langmuir, Freundlich and Temkin isotherm models were used. The adequacy of the isotherm equation was determined based on the R^2 correlation coefficients.

Langmuir isotherm: The Langmuir model assumes that the adsorbate will only form one layer on the adsorbent's surface. In addition, the adsorption sites are all energetically equivalent (homogeneous) and there is no interaction between adjacent adsorbed molecules [37]. The Langmuir isotherm equation is given by:

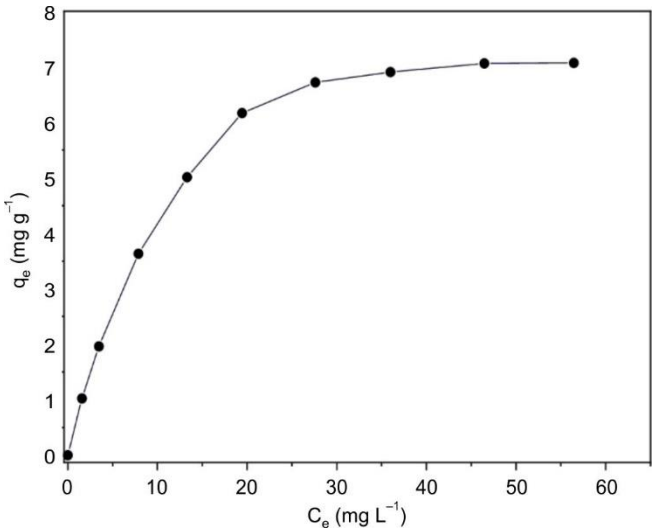

Fig. 18. The equilibrium adsorption isotherm of MV2B onto SS

$$\frac{C_e}{q_e} = \frac{1}{q_m K_L} + \frac{1}{q_m} C_e \quad (6)$$

where C_e is the equilibrium concentration (mg/L); q_e is the equilibrium amount adsorbed per unit weight of SS (mg/g), q_m the monolayer capacity of the adsorbent (the theoretical maximum adsorption capacity of adsorbate per unit mass of adsorbent (mg/g) and K_L is the Langmuir adsorption constant (L/mg). The values of q_m and K_L can be determined from the slope and the intercept of the linear plot (Fig. 19) of the experimental data C_e/q_e *versus* C_e (shown in Table-2).

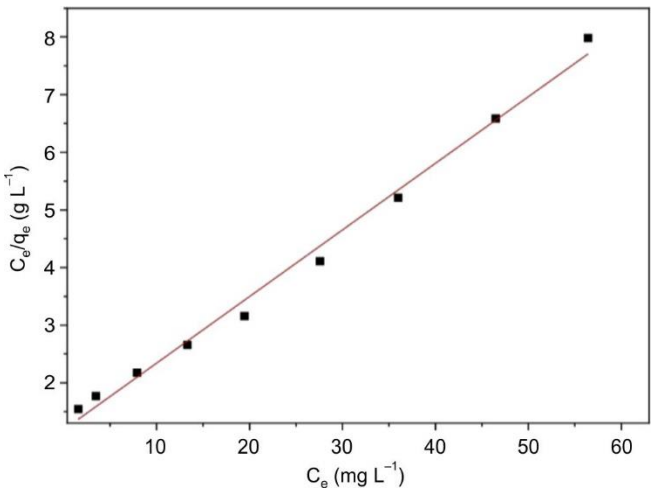

Fig. 19. Langmuir linear adsorption isotherm of MV2B onto SS

Freundlich isotherm: The Freundlich model is based on the adsorption onto heterogeneous surfaces supporting sites with variable affinities. It suggests that the more significant binding sites are occupied first and the binding strength decreases with the increasing degree of site occupation. It is expressed by the empirical equation [38]:

$$\ln q_e = \ln K_F + \frac{1}{n} \ln C_e \quad (7)$$

where K_F represents the Freundlich adsorption constant related to the adsorption capacity of the adsorbent (mg/g)

TABLE-2
LANGMUIR, FREUNDLICH AND TEMKIN ISOTHERM CONSTANTS FOR ADSORPTION OF MV2B ONTO SS

Langmuir			Freundlich			Temkin		
q_m (mg/g)	K_L	R^2	n	K_F	R^2	B_T	K_T	R^2
8.828	0.100	0.992	1.882	1.003	0.935	1.875	1.005	0.974

$(L/mg)^{1/n}$ and n reflects the adsorption intensity. The values of K_F and n (Table-2) were calculated from the intercept and slope of the plot ln q_e *versus* ln C_e (Fig. 20). The heterogeneity factor n provides insights into the nature of the adsorption process. If n = 1: the adsorption is linear; if n < 1: it is a chemical adsorption and if n > 1: it is a physical adsorption. The obtained values of n = 1.882 suggest that the adsorption is physical and the experimental data preferably fit the Langmuir isotherm (R^2 = 0.992). The R^2 value for the Freundlich model was 0.935 [38].

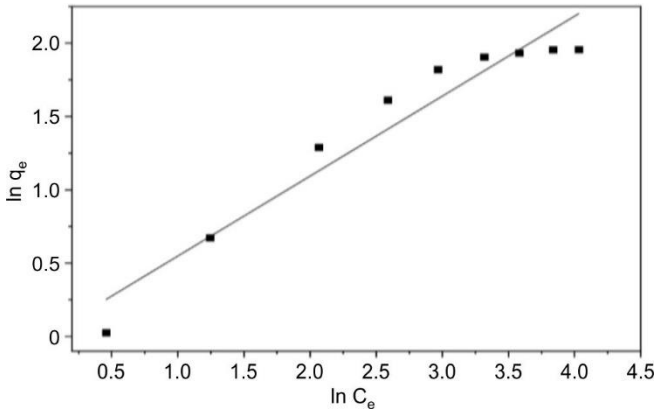

Fig. 20. Freundlich linear adsorption isotherm of MV2B onto SS

Temkin isotherm: The proposed model assumes that the heat of adsorption for all molecules in the layer decreases linearly with surface coverage due to adsorbent-adsorbate interactions. The linear form of Temkin isotherm is expressed as [39]:

$$q_e = B_T \ln K_T + B_T \ln C_e \quad (8)$$

where B_T is the Temkin constant associated with the heat of adsorption; and K_T is the Temkin equilibrium binding constant (L/mg). The constants B_T and K_T (Table-2) can be determined by plotting q_e *versus* Ln C_e (Fig. 21).

However, the R^2 value of 0.974 is not bad, nevertheless, the Langmuir model (R^2 = 0.992) is better than the Temkin's model for describing the equilibrium isotherm data for the adsorption of MV2B onto SS. It can be seen from these results that the maximum adsorption capacity value of SS (q_m = 8.828 mg/g) is higher than those of many adsorbents such as raw *Posidonia oceanica* fibres (q_m = 5.56 mg/g) [40] and Orange peel (q_m = 3.26 mg/g) [41] for removing methylene blue and rhodamine B.

Thermodynamic parameters of adsorption: The estimation of thermodynamic parameters was conducted to ascertain the spontaneity of the reaction. This was achieved by plotting ln K_d *versus* 1/T within a temperature range of 293.15-323.15 K, as illustrated in Fig. 22. The change in standard Gibb's free energy (ΔG^o) is expressed by eqns. 9 and 10:

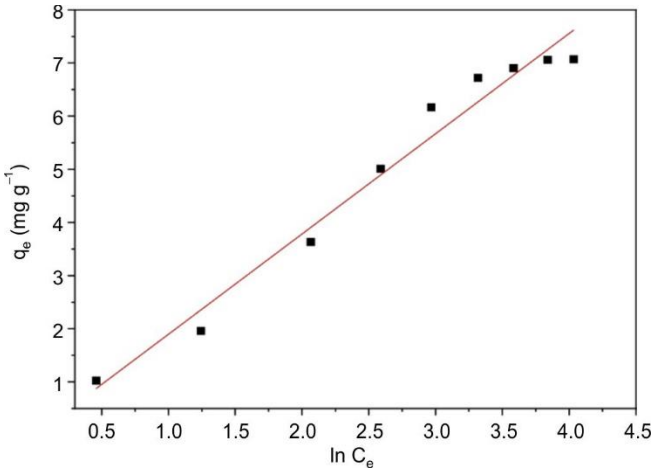

Fig. 21. Temkin linear adsorption isotherm of MV2B onto SS

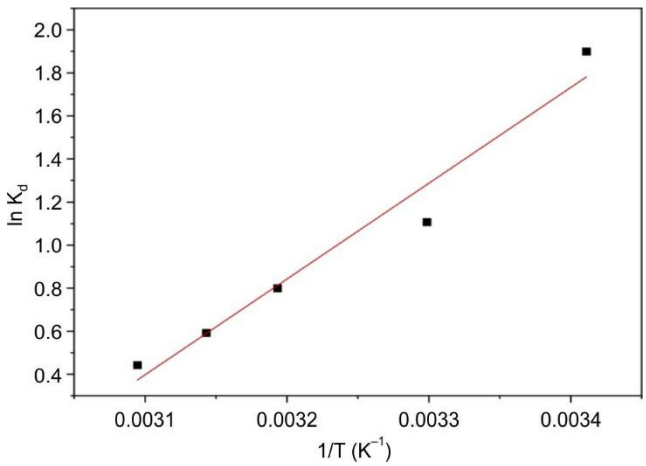

Fig. 22. Plot of ln K_d *versus* 1/T for MV2B adsorption onto SS

$$\Delta G^o = \Delta H^o - T\Delta S^o \quad (9)$$

$$\Delta G^o = -RT \ln K_d \quad (10)$$

The change in standard entropy ΔS^o and standard enthalpy ΔH^o of the sorption process were deduced from the Van't Hoff equation [42] and expressed as:

$$\ln K_d = \frac{\Delta S^o}{R} - \frac{\Delta H^o}{R} \times \frac{1}{T} \quad (11)$$

The thermodynamic equilibrium constant K_d of the adsorption process is defined as:

$$K_d = \frac{C_{a\,ads}}{C_e} = \frac{C_o - C_e}{C_e} \quad (12)$$

where C_{aads} is mg of adsorbate adsorbed per litre; C_o is the initial dye concentration (mg/L); and C_e is the equilibrium concentration of solution (mg/L) [43].

TABLE-3
THERMODYNAMIC PARAMETERS OF ADSORPTION OF MV2B ONTO SS

Adsorbent	ΔH^o (kJ/mol)	ΔS^o (J/mol K)	Temp. (K)	ΔG^o (kJ/mol)	R^2
SS	-36.984	-111.347	293.15	–4.343	0.960
			303.15	–3.229	
			313.15	–2.116	
			323.15	–1.002	

According to the eqn. 11, the values of enthalpy change ΔH^o and entropy change ΔS^o were calculated from the slope and intercept of the plot of ln K_d *versus* 1/T. As depicted in Table-3, the negative values of ΔG^o and ΔH^o indicate the spontaneous and exothermic nature of the MV2B dye adsorption process. Due to the low values of ΔH and ΔG, the process corresponds to physisorption, which involves weak, non-specific interactions such as van der Waals forces. Furthermore, the negative value of ΔS^o indicated a decrease in randomness within the system at the solid/solute interface during the adsorption of MV2B onto SS.

Conclusion

This study was carried out to investigate the potential of food waste as an adsorbent for the removal of the cationic dye methyl violet 2B (MV2B) from the contaminated water. The snail shell (SS) adsorbent was thoroughly characterized using FTIR, SEM, TGA/DTA and XRD techniques. FTIR confirmed the successful adsorption of the cationic dye onto SS. SEM analysis revealed a stratified lamellar structure with small, irregular particles offering accessible adsorption sites. TGA/DTA results showed high thermal stability, while XRD identified $CaCO_3$ as the main component. The SS adsorbent demonstrated high adsorption efficiency (up to 93.63%). Kinetic and isotherm studies indicated that the adsorption followed a pseudo-second-order model and conformed to the Langmuir isotherm. Thermodynamic analysis confirmed the process to be exothermic and spontaneous. These findings demonstrated that snail shell, a form of food waste, is a promising, cost-effective and eco-friendly adsorbent for the removal of MV2B from the aqueous systems, underscoring its potential in sustainable water detoxification applications.

CONFLICT OF INTEREST

The authors declare that there is no conflict of interests regarding the publication of this article.

REFERENCES

1. I. Azreen, J.N. Syufiana, R.J. Fletcher and Y.A. Zahrim, in eds.: N. Wan, Revisited Coagulation-Flocculation-Nanofiltration for Dye Removal, In: Water Resources Management and Water Pollution Control. ISWPT 2023. Environmental Science and Engineering, Springer, Cham, pp. 83–89 (2024).
2. C.E. Enenebeaku, I.C. Ukaga, J.N. Okorocha and B.I. Onyeachu, *Int. Lett. Chem. Phys. Astron.*, **80**, 17 (2018); https://doi.org/10.56431/p-7a2n7i
3. E.O. Jatto, I.O. Asia, F. Egharevba and C.J. Ewansiha, *Water-Energy Nexus*, **3**, 95 (2020); https://doi.org/10.1016/j.wen.2020.06.001
4. J. Gupta and M. Agarwal, *Biofuels*, **10**, 315 (2019); https://doi.org/10.1080/17597269.2016.1200862
5. K.F. Kayani, S.J. Mohammed, M.S. Mustafa and S.B. Aziz, *Mater. Adv.*, **6**, 5391 (2025); https://doi.org/10.1039/D5MA00572H
6. A. Mittal, V. Gajbe and J. Mittal, *J. Hazard. Mater.*, **150**, 364 (2008); https://doi.org/10.1016/j.jhazmat.2007.04.117
7. O.T. Ogunmodede, O.L. Adebayo and A.A. Ojo, *Int. Lett. Chem. Phys. Astron.*, **39**, 35 (2014); https://doi.org/10.56431/p-8rzvmp
8. R. K. Abbas and M.A. AL-Da'amy, *IOP Conf. Ser.: Mater. Sci. Eng.*, **928**, 052011 (2020); https://doi.org/10.1088/1757-899X/928/5/052011
9. M. Alsuhybani, M. Aleid, R. Alzidan, K. Bin Bander and A. Alrehaili, *Heliyon*, **10**, e36731 (2024); https://doi.org/10.1016/j.heliyon.2024.e36731
10. H. Fatimah, P. Taba, St. Fauziah, A. Karim, S. Liong, S. Kasim, S. Sahrul and N.A. Pardan, *J. Ecol. Eng.*, **26**, 73 (2025); https://doi.org/10.12911/22998993/200503
11. A. Kadam, J. Jang, S.-R. Lim and D.S. Lee, *Theor. Found. Chem. Eng.*, **54**, 655 (2020); https://doi.org/10.1134/S0040579520040193
12. M.A. Al-Da'amy and R.Q. Al-Shemary, *J. Glob. Pharma Technol.*, **10**, 422 (2018).
13. J. Aguilar-Rosero, M.E. Urbina-López, B.E. Rodríguez-González, S.X. León-Villegas, I.E. Luna-Cruz and D.L. Cárdenas-Chávez, *Appl. Sci.*, **12**, 2740 (2022); https://doi.org/10.3390/app12052740
14. Y. Saghir, A. Chaoui, S. Farsad, A. Ben Hamou, A. Amjlef, M. Benafqir, N. El Alem and M. Ez-zahery, *Mater. Adv.*, **6**, 4857 (2025); https://doi.org/10.1039/D5MA00253B
15. N.T.H. Nhung, V.D. Long and T. Fujita, *Materials*, **16**, 1095 (2023); https://doi.org/10.3390/ma16031095
16. R. Yadav, A.K. Sharma and A. Yadav, *Asian J. Chem.*, **36**, 1265 (2024); https://doi.org/10.14233/ajchem.2024.31398
17. A.A. Adaramaja, A. Bamisaye, S.M. Abati, K.A. Adegoke, M.O. Adesina, A.R. Ige, O. Adeleke, M.A. Idowu, A.K. Oyebamiji and O.S. Bello, *RSC Adv.*, **14**, 12703 (2024); https://doi.org/10.1039/D4RA01074D
18. F.B. Zwier, M.A. Al-Da'amy and E.T. Kareem, *Baghdad Sci. J.*, **21**, 1296 (2024); https://doi.org/10.21123/bsj.2023.8311
19. W.J. Zhao, D.W. Liu, H.S. Li, Q.C. Feng, G.Y. Xu, J.J. Yuan and X.D. Jia, *Adv. Mat. Res.*, **616**, 614 (2012); https://doi.org/10.4028/www.scientific.net/AMR.616-618.614
20. M.S. Tizo, L.A.V. Blanco, A.C.Q. Cagas, B.R.B. Dela Cruz, J.C. Encoy, J.V. Gunting, R.O. Arazo and V.I.F. Mabayo, *Sustain. Environ. Res.*, **28**, 326 (2018); https://doi.org/10.1016/j.serj.2018.09.002
21. V. Aravind and K.P. Elango, *Indian J. Chem. Technol.*, **13**, 476 (2006).
22. A. Hossain, S.R. Bhattacharyya and G. Aditya, *Environ. Technol. Innov.*, **4**, 82 (2015); https://doi.org/10.1016/j.eti.2015.05.001
23. I.B. Laskar, K. Rajkumari, R. Gupta, S. Chatterjee, B. Paul and L. Rokhum, *RSC Adv.*, **8**, 20131 (2018); https://doi.org/10.1039/C8RA02397B
24. G.D. Silcox, J.C. Kramlich and D.W. Pershing, *Ind. Eng. Chem. Res.*, **28**, 155 (1989); https://doi.org/10.1021/ie00086a005
25. M. Sattar, M.Sc. Thesis, Adsorption of Crystal Violet on Commercial Activated Carbon and Activated Carbon Obtained from Bagasse. Prince of Songkla University, Songkhla, Thailand pp. 2–25 (2010).
26. M.R.R. Kooh, M.K. Dahri and L.B. Lim, *Appl. Water Sci.*, **7**, 3573 (2017); https://doi.org/10.1007/s13201-016-0496-y

27. N.K. Amin, *J. Hazard. Mater.*, **165**, 52 (2009); https://doi.org/10.1016/j.jhazmat.2008.09.067
28. S. Chowdhury, S. Chakraborty and P.D. Saha, *Waste Biomass Valoriz.*, **4**, 655 (2013); https://doi.org/10.1007/s12649-012-9139-1
29. L.R. Bonetto, F. Ferrarini, C. De Marco, J. Crespo, R. Guégan and M. Giovanela, *J. Water Process Eng.*, **6**, 11 (2015); https://doi.org/10.1016/j.jwpe.2015.02.006
30. S. Lagergren, *K. Sven. Vetenskapsakad. Handl*, **24**, 1 (1898).
31. H. Patel and R. Vashi, *J. Environ. Eng. Landsc. Manag.*, **21**, 36 (2013); https://doi.org/10.3846/16486897.2012.671772
32. J. Rahchamani, H.Z. Mousavi and M. Behzad, *Desalination*, **267**, 256 (2011); https://doi.org/10.1016/j.desal.2010.09.036
33. W.J. Weber Jr. and J.C. Morris, *J. Sanit. Engrg. Div.*, **89**, 31 (1963); https://doi.org/10.1061/JSEDAI.0000430
34. M. Doğan, Y. Özdemir and M. Alkan, *Dyes Pigments*, **75**, 701 (2007); https://doi.org/10.1016/j.dyepig.2006.07.023
35. I.D. Mall, V.C. Srivastava and N.K. Agarwal, *Dyes Pigments*, **69**, 210 (2006); https://doi.org/10.1016/j.dyepig.2005.03.013
36. M.A. Al-Ghouti and D.A. Da'ana, *J. Hazard. Mater.*, **393**, 122383 (2020); https://doi.org/10.1016/j.jhazmat.2020.122383
37. J. Zolgharnein, F. Gholami, N. Asanjarani, P. Zolgharnein and G. Azimi, *Sep. Sci. Technol.*, **49**, 752 (2014); https://doi.org/10.1080/01496395.2013.862547
38. A.L. Cazetta, A.M. Vargas, E.M. Nogami, M.H. Kunita, M.R. Guilherme, A.C. Martins, T.L. Silva, J.C.G. Moraes and V.C. Almeida, *Chem. Eng. J.*, **174**, 117 (2011); https://doi.org/10.1016/j.cej.2011.08.058
39. A.O. Dada, J. Ojediran, A.A. Okunola, F. Dada, A. Lawal, A. Olalekan and O. Dada, *Int. J. Mech. Eng. Technol.*, **10**, 1048 (2019).
40. V. Vadivelan and K.V. Kumar, *J. Colloid Interface Sci.*, **286**, 90 (2005); https://doi.org/10.1016/j.jcis.2005.01.007
41. A.A. Oyekanmi, A. Ahmad, K. Hossain and M. Rafatullah, *J. Mol. Liq.*, **281**, 48 (2019); https://doi.org/10.1016/j.molliq.2019.02.057
42. A.P. Rawat, V. Kumar and D.P. Singh, *Sep. Sci. Technol.*, **55**, 907 (2020); https://doi.org/10.1080/01496395.2019.1580732
43. T.M. Tamer, W.A.A. Sadik, R.A. Elady, A.M. Omer, M.M. Abd-Ellatif and M.S. Mohy-Eldin, *Desalination Water Treat.*, **317**, 100122 (2024); https://doi.org/10.1016/j.dwt.2024.100122